crystals

Article

Crystal Structure, Raman Spectrum and Tl^{+} Lone-Pair Luminescence of Thallium(I) Dodecahydro-Monocarba-*closo*-Dodecaborate $Tl[CB_{11}H_{12}]$

Kevin U. Bareiß [1], David Enseling [2], Thomas Jüstel [2] and Thomas Schleid [1,*]

[1] Institute for Inorganic Chemistry, University of Stuttgart, Pfaffenwaldring 55, 70569 Stuttgart, Germany
[2] Department of Chemical Engineering, FH Münster—University of Applied Sciences, Stegerwaldstraße 39, 48565 Steinfurt, Germany
* Correspondence: schleid@iac.uni-stuttgart.de

Abstract: $Tl[CB_{11}H_{12}]$ was prepared with a reaction of $Tl_2[CO_3]$ with the acid of the monocarba-*closo*-dodecaborate anion $(H_3O)[CB_{11}H_{12}]$ in aqueous solution as prismatic colorless single crystals by isothermal evaporation from the clear brine. It crystallizes in a monoclinic primitive structure with the space group $P2_1/c$ (a = 685.64(3) pm, b = 1978.21(9) pm, c = 1006.89(5) pm, β = 132.918(3)° for Z = 4), which can be derived from the halite-type arrangement if the *closo*-carbaborate cages are considered as spheres. Due to the different atoms in the $[CB_{11}H_{12}]^{-}$ anion, $Tl[CB_{11}H_{12}]$ features interesting $C–H^{\delta+} \cdots {}^{\delta-}H–B$ interactions near to non-classical hydrogen bridges ("dihydrogen bonds") and exhibits considerably different luminescence properties compared to regular *closo*-hydroborates, such as $Tl_2[B_{10}H_{10}]$, $Tl_2[B_{12}H_{12}]$ and $Tl_3Cl[B_{12}H_{12}]$. $Tl[CB_{11}H_{12}]$ shows strong photoluminescence (PL) at 390 nm, while the excitation bands for this broad band are located at 245 and 280 nm. It is caused by an interconfigurational $[Xe]4f^{14}5d^{10}6s^{2}$ ($^{3}P_{1}$) to $[Xe]4f^{14}5d^{10}6s^{1}6p^{1}$ ($^{1}S_{0}$) transition, which is also known as lone-pair luminescence. The quantum yield is rather low (<10 %), which is likely caused by the rather large Stokes shift. In addition, temperature-dependent emission spectra were recorded to determine the thermal quenching curve and the respective quenching temperature.

Keywords: carborates; thallium(I) salts; monocarba-*closo*-hydroborates; single-crystal X-ray diffraction; Raman spectra; photoluminescence; stokes shift; thermal quenching

check for updates

Citation: Bareiß, K.U.; Enseling, D.; Jüstel, T.; Schleid, T. Crystal Structure, Raman Spectrum and Tl^{+} Lone-Pair Luminescence of Thallium(I) Dodecahydro-Monocarba-*closo*-Dodecaborate $Tl[CB_{11}H_{12}]$. *Crystals* **2022**, *12*, 1840. https://doi.org/10.3390/cryst12121840

Academic Editor: Simon Duttwyler

Received: 29 November 2022
Accepted: 9 December 2022
Published: 16 December 2022

1. Introduction

Dodecahydro-monocarba-*closo*-dodecaborate monoanions $[CB_{11}H_{12}]^{-}$ feature the same three-dimensional aromaticity like regular *closo*-dodecaborate dianions $[B_{12}H_{12}]^{2-}$, which explains the striking thermodynamical stability of such species. Despite their high stability, which makes them easy to handle under atmospheric conditions, structural research on binary inorganic salts with $[CB_{11}H_{12}]^{-}$ anions is still rather uncommon. Up to now only the crystal structures of the alkali-metal salts $A[CB_{11}H_{12}]$ (A = Li–K and Cs) [1–4] have been reported, of which $Li[CB_{11}H_{12}]$ and $Na[CB_{11}H_{12}]$ were moved into the research focus due to their high cationic conductivity [1,2]. Their crystal structures are often based on simple structure types like the *anti*-fluorite-type for $[B_{12}H_{12}]^{2-}$ containing salts $A_2[B_{12}H_{12}]$ and the halite-type for those with $[CB_{11}H_{12}]^{-}$ anions. Contrary to the *closo*-dodecaborates, monocarba-*closo*-dodecaborates do not crystallize within the cubic crystal system at room temperature, although they typically feature phase transitions into highly disordered cubic phases, as soon as the rotational barrier for the $[CB_{11}H_{12}]^{-}$ anion is thermally abrogated [1–3,5].

In this study, we present the synthesis and characterization of the previously unknown thallium(I) salt $Tl[CB_{11}H_{12}]$. As the combination of cations with electronic lone pairs and *closo*-hydroborate anions provided salts with interesting photoluminescence properties, such as $Tl_2[B_{12}H_{12}]$ [6,7], $Tl_2[B_{10}H_{10}]$ [6], and $Tl_3Cl[B_{12}H_{12}]$ [8], already it was a matter of particular interest to see, how the luminescence properties of Tl^+ will change, when a carbon atom is substituted into the *closo*-borate cage within the $[CB_{11}H_{12}]^-$ counter anion.

2. Materials and Methods

2.1. Synthesis

Thallium(I) dodecahydro-monocarba-*closo*-dodecaborate $Tl[CB_{11}H_{12}]$ was prepared with a reaction of thallium(I) oxocarbonate $Tl_2[CO_3]$ (Merck-Schuchardt, Hohenbrunn, Germany, 99 %) with the acid of the monocarba-*closo*-dodecaborate anion $(H_3O)[CB_{11}H_{12}]$ in an aqueous solution. The free acid $(H_3O)[CB_{11}H_{12}]$ itself was accessed by passing a concentrated aqueous solution of $Cs[CB_{11}H_{12}]$ (Katchem, Prague, Czech Republic, 97 %) solution through a column filled with the highly acidic cation exchange resin Amberlite IR-120 (Merck, Darmstadt, Germany). Colorless prismatic single crystals of $Tl[CB_{11}H_{12}]$ were obtained by isothermal evaporation from the clear solution of the initial reaction mixture.

2.2. Single-Crystal X-ray Diffraction

The selected single-crystal specimen of $Tl[CB_{11}H_{12}]$ was prepared in a 0.1 mm glass capillary and measured on a κ-CCD four-circle single-crystal X-ray diffractometer (Bruker-Nonius, Delft, Netherlands) at room temperature. The diffractometer is equipped with a 1K CCD detector, a Mo-K_α X-ray tube and a graphite monochromator. Structure solution and refinement were carried out on basis of the SHELX-2013 program package [9].

2.3. Optical Spectroscopy

Raman-spectroscopic measurements were carried out on a XploRA Raman spectroscope (Horiba Jobin Yvon, Bensheim, Germany) equipped with a BX51 polarisation microscope (Olympus, Hamburg, Germany) and two solid-state lasers with wavelenghts of 532 nm (25 mW) and 638 nm (24 mW). For hardware calibration, the T_{2g} mode (521 cm^{-1}) of a silicon wafer was used.

The emission and excitation spectrum at room temperature as well as the temperature-dependent emission spectra of $Tl[CB_{11}H_{12}]$ were collected using a fluorescence spectrometer FLS920 (Edinburgh Instruments, Livingston, UK) equipped with a 450 W Xenon discharge lamp (Osram, Munich, Germany). Additionally, a mirror optic for powder samples was used. The detection served a R2658P single-photon-counting photomultiplier tube (Hamamatsu,Herrsching am Ammersee, Germany). Temperature-resolved spectra were recorded by using a cryostat "MicrostatN" from Oxford Instruments (Abingdon, UK), wherein the powder sample was mounted.

For the determination of the reflection spectrum, the sample was placed into a $Ba[SO_4]$ coated integrating sphere as part of an FLS920 (Edinburgh Instruments) spectrometer equipped with a 450 W Xenon lamp, and a cooled (–20 °C) single-photon counting photomultiplier (Hamamatsu R928). $Ba[SO_4]$ was also used as a white reflectance standard. The excitation and emission band widths were 10.00 and 0.06 nm, respectively. The applied step width was 1 nm and the integration time was 0.5 s.

3. Results and Discussion

3.1. Crystal Structure

The thallium(I) dodecahydro-monocarba-*closo*-dodecaborate $Tl[CB_{11}H_{12}]$ crystallizes in the monoclinic space group $P2_1/c$ with lattice parameters of a = 685.64(3) pm, b = 1978.21(9) pm, c = 1006.89(5) pm and β = 132.918(3)° for four formula units per unit cell. Further crystallographic data for the determination of the structure are given in Table 1 and the corresponding atom sites, thermal displacement parameters and selected inter-atomic distances can be found in Tables 2–4.

Table 1. Crystallographic data of $Tl[CB_{11}H_{12}]$ and their determination.

empirical formula	$Tl[CB_{11}H_{12}]$
crystal system	monoclinic
space group	$P2_1/c$ (no. 14)
lattice parameters	
a/pm	685.64(3)
b/pm	1978.21(9)
c/pm	1006.89(5)
$\beta/°$	132.918(3)
number of formula units, Z	4
calculated density, D_x/g cm^{-3}	2.307
molar volume, V_m/cm^3 mol^{-1}	150.57
diffractometer	κ-CCD (Bruker-Nonius)
radiation wavelength	Mo-K$_\alpha$: $\lambda = 71.07$ pm
diffraction limit, $2\Theta_{max}/°$	54.92
hkl range, $\pm h_{\mathrm{max}}$, $\pm k_{\mathrm{max}}$, $\pm l_{\mathrm{max}}$	8, 25, 12
$F(000)/e^-$	616
absorption coefficient, μ/mm^{-1}	16.07
extinction coefficient, ε	0.0114(5)
measured reflections	17,476
unique reflections	2283
R_{int}, R_σ	0.064, 0.038
R_1, wR_2, GooF	0.034, 0.081, 1.028
Residual electron density (max., min. / e^- 10^{-6} pm^{-3})	1.31, –1.14
CCDC number	2221677

Table 2. Fractional atomic coordinates and equivalent isotropic displacement parameters of $Tl[CB_{11}H_{12}]$ (all atoms occupy the general Wyckoff site *4e*).

Atom	*x/a*	*y/b*	*z/c*	U_{eq}/pm^2
Tl	0.62389(6)	0.094958(15)	0.73978(4)	627(2)
C1 ǀ B11 *	0.4456(14)	0.1820(3)	0.0867(9)	501(2)
H11	0.380	0.218	−0.021	601
C2 ǀ B12 *	0.7656(15)	0.1829(4)	0.2906(10)	484(2)
H12	0.916	0.218	0.322	581
B1	0.5088(16)	0.2123(4)	0.2735(10)	493(2)
H1	0.489	0.266	0.293	592
B2	0.2288(14)	0.1606(4)	0.1112(10)	447(2)
H2	0.025	0.180	0.024	536
B3	0.3194(14)	0.1016(4)	0.0286(10)	459(2)
H3	0.175	0.083	−0.112	551
B4	0.6534(15)	0.1166(4)	0.1404(10)	468(2)
H4	0.727	0.108	0.073	562
B5	0.8532(15)	0.1012(4)	0.3737(10)	489(2)
H5	1.057	0.082	0.459	587
B6	0.7650(15)	0.1614(4)	0.4569(9)	489(2)
H6	0.912	0.181	0.596	587
B7	0.4234(14)	0.1461(3)	0.3429(10)	414(2)
H7	0.347	0.156	0.408	497
B8	0.3074(15)	0.0776(4)	0.1926(10)	443(2)
H8	0.156	0.042	0.160	665
B9	0.5716(13)	0.0500(3)	0.2102(9)	417(2)
H9	0.592	−0.003	0.190	500
B10	0.6406(15)	0.0775(4)	0.4084(10)	437(2)
H10	0.707	0.043	0.517	524

* These C-atom sites are both occupied by carbon and boron at an equivalent 1:1 molar ratio. Hydrogen atoms have been refined with a distance of 110 pm to their respective covalent binding partners (C and B) at 1.2 times of their equivalent isotropic displacement parameters using the SHELX command AFIX 153 [10,11].

Table 3. Selected intramolecular distances (d/pm) within the $[CB_{11}H_{12}]^-$ anion in $Tl[CB_{11}H_{12}]$.

C1 ǀ B11	−C2 ǀ B12	170.1(10)	C2 ǀ B12	−C1 ǀ B11	170.1(10)
	−B3	171.1(9)		−B5	172.8(11)
	−B4	171.7(10)		−B6	173.0(10)
	−B2	171.7(9)		−B4	173.7(10)
	−B1	172.4(9)		−B1	174.7(10)
	−H11	110		−H12	110
B1	−C1 ǀ B11	172.5(9)	B2	−C1 ǀ B11	171.7(9)
	−C2 ǀ B12	174.7(10)		−B8	174.9(10)
	−B6	175.9(11)		−B7	175.1(10)
	−B7	176.3(9)		−B1	176.9(10)
	−B2	176.9(10)		−B3	177.3(10)
	−H1	110		−H2	110
B3	−C1 ǀ B11	171.0(9)	B4	−C1 ǀ B11	171.7(10)
	−B9	175.2(10)		C2 ǀ B12	173.8(10)
	−B4	175.7(10)		−B9	175.4(10)
	−B2	177.3(10)		−B3	175.7(10)
	−B8	177.4(10)		−B5	176.1(10)
	−H3	110		−H4	110
B5	−C2 ǀ B12	172.9(11)	B6	−C2 ǀ B12	173.0(10)
	−B4	176.1(10)		−B1	175.9(11)
	−B9	177.1(10)		−B10	177.6(10)
	−B10	177.8(10)		−B5	178.2(10)
	−B6	178.2(10)		−B7	179.8(10)
	−H5	110		−H6	110
B7	−B2	175.1(10)	B8	−B2	174.9(10)
	−B1	176.3(10)		−B7	176.6(10)
	−B8	176.7(10)		−B3	177.3(10)
	−B10	177.6(10)		−B9	178.0(9)
	−B6	179.8(10)		−B10	178.4(10)
	−H7	110		−H8	110
B9	−B3	175.2(10)	B10	−B6	177.5(10)
	−B4	175.5(10)		−B7	177.6(10)
	−B5	177.1(10)		−B5	177.8(10)
	−B8	178.0(9)		−B8	178.4(10)
	−B10	179.3(9)		−B9	179.3(9)
	−H9	110		−H10	110

Table 4. Distances (d/pm) between the Tl^+ cations and coordinatively relevant hydrogen atoms of the $[CB_{11}H_{12}]^-$ anions in $Tl[CB_{11}H_{12}]$ up to 400 pm.

Tl	−H9	272.5
	−H7	275.0
	−H2	280.7
	−H10	285.4
	−H5	286.3
	−H4	293.3
	−H8	293.4
	−H3	298.1
	−H1	306.5
	··· H10	335.4
	··· H8	335.9
	··· H6	357.6

Due to the quite similar atomic form factors of carbon and boron [12], they cannot be distinguished in the Fourier syntheses unambigously, which is why the position of the single carbon atom of the $[CB_{11}H_{12}]^-$ anion had to be determined by the structural differences between the different atom sites within the $[CB_{11}H_{12}]^-$ cage as shown in Figure 1. So C1 shows the shortest intramolecular distances of 170 to 172 pm within the icosahedron, followed by C2 with values between 170 and 175 pm, whereas the distances between the boron atoms B2–B10 range from 175 to 180 pm, which is rather typical for B–B bond lengths in *closo*-dodecaborates. In addition to these differences in bond lengths, the hydrogen atoms H11 and H12 at the corresponding C1 and C2 atoms do not show any Tl–H interactions, hence predicting a reciprocally polarized $C^{\delta-}$–$H^{\delta+}$ bond in comparison with the $B^{\delta+}$–$H^{\delta-}$ bonds. Therefore, it can be assumed that only one carbon site of the carbaborate cage is occupied at a time, due to a orientational disorder of the $[CB_{11}H_{12}]^-$ anion within the crystal structure. This effect was observed for measurements both at room temperature as well as at −196 °C, suggesting a static instead of a dynamic disorder.

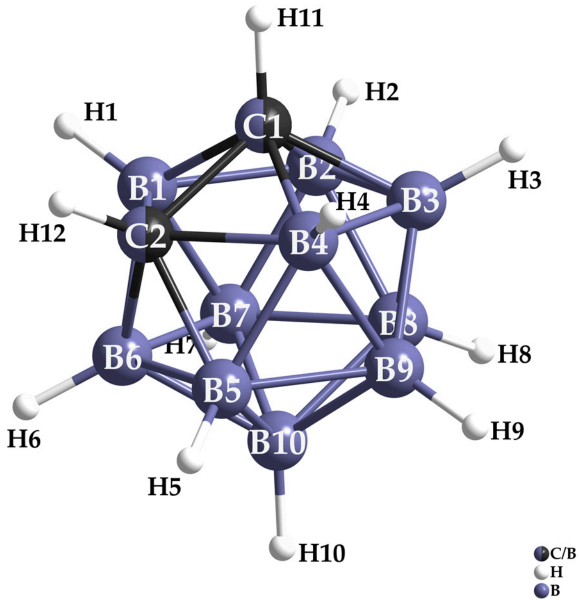

Figure 1. Atom-numbering scheme of the $[CB_{11}H_{12}]^-$ anion in $Tl[CB_{11}H_{12}]$ with the atomic positions C1, C2, B1–B10, H1–H10, H11 and H12, where due to the orientational disorder only one of the two carbon sites is occupied at a time.

The differences in coordination of the individual hydrogen atoms of the $[CB_{11}H_{12}]^-$ anion are shown in Figure 2. Clearly visible are the missing Tl–H contacts at the two possible carbon sites, but also the fact that three Tl^+ cations are coordinated via edges or faces of the pseudo-icosahedral cages, but the remaining three on the top and at the right hand side of Figure 2 graft only terminally. The resulting distorted octahedral coordination of the $[CB_{11}H_{12}]^-$ anion by Tl^+ cations thus divides into three more distant terminal Tl^+ cations with Tl–H distances from 286 to 307 pm with B–H–Tl angles of 138 to 152° and three closer Tl^+ cations coordinated via edges (or faces) at distances from 272 to 298 pm, but much smaller angles of 109 to 116°. The three closer Tl^+ cations always show a third contact to the $[CB_{11}H_{12}]^-$ anion, which is emphasized as fragmented bond each due to the very long Tl···H distances of 335–358 pm.

Regarding the coordination environment of the singular Tl^+ cation in $Tl[CB_{11}H_{12}]$ (Figures 3 and 4), it also shows a distorted octahedral coordination of six $[CB_{11}H_{12}]^-$ anions leading to a simple *AB* structure, if the $[CB_{11}H_{12}]^-$ anions are treated as spheres, which is why the structure can be deduced from the NaCl-type arrangement. Figure 5 shows the resulting extended unit cell within the crystal structure of $Tl[CB_{11}H_{12}]$, in which bilayers of $[CB_{11}H_{12}]^-$ anions with intercalated Tl^+ cations stacked along [010] are found. These bilayers feature surprisingly short H···H contacts of 247 and 258 (2×) pm that all belong to C–$H^{\delta+}$ ··· ${}^{\delta-}$H–B contacts. These distances are significantly longer than non-classical dihydrogen bonds covering a typical range between 170 and 220 pm [13–15], however, but especially 248 pm as the shortest of them appear very close to twice of the van der Waals radii of hydrogen equaling 240 pm [16] and thus should yield a non-negligible electrostatic interaction. This also supports the proposed orientational disorder of the $[CB_{11}H_{12}]^-$

anion, as only the positively partial charged hydrogen atoms bound to carbon show such short contacts.

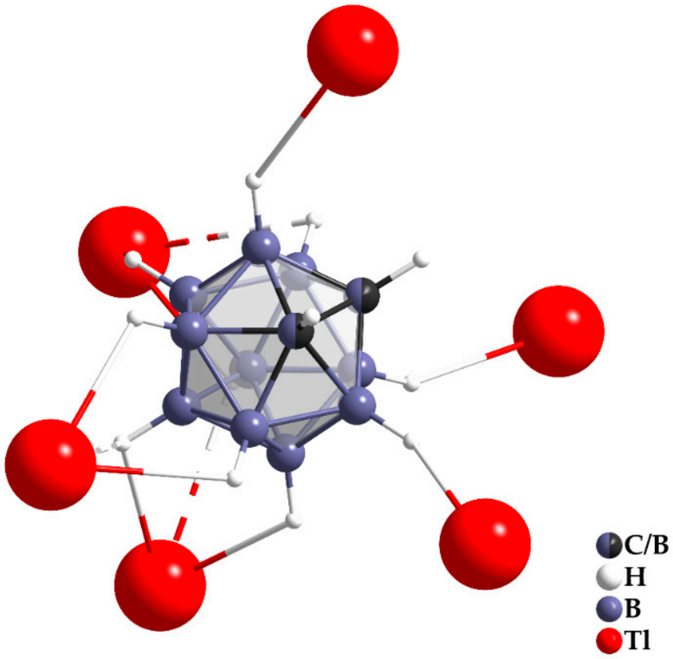

Figure 2. Heavily distorted octahedral coordination sphere of the anionic $[CB_{11}H_{12}]^-$ cage by six Tl^+ cations in the crystal structure of $Tl[CB_{11}H_{12}]$.

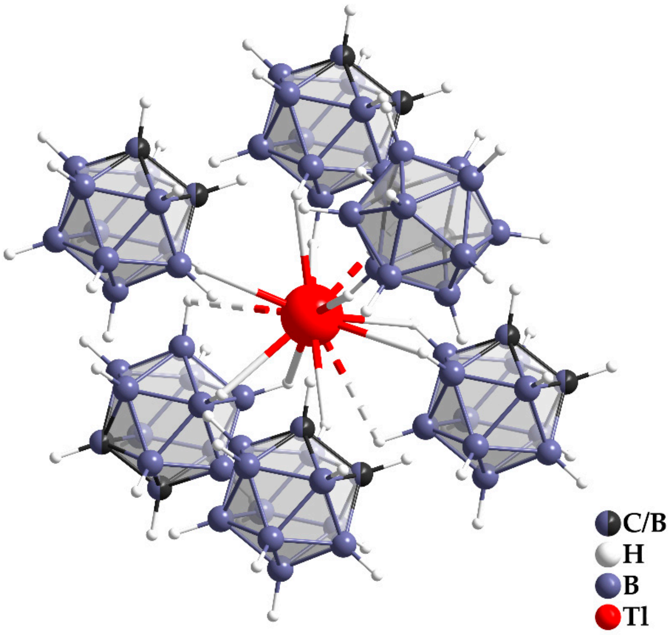

Figure 3. Coordination sphere of the singular Tl^+ cation in the crystal structure of $Tl[CB_{11}H_{12}]$ by twelve hydrogen atoms (C.N. = 9 + 3) of six monocarbaborate anions $[CB_{11}H_{12}]^-$.

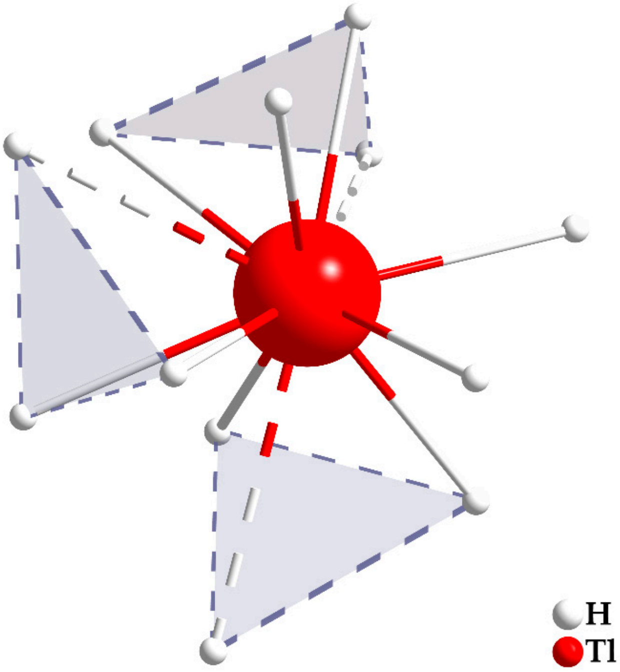

Figure 4. Reduced coordination scheme of the Tl^{+} cation by hydrogen in the crystal structure of $Tl[CB_{11}H_{12}]$ confined to the first coordination sphere of atoms with triangular planes to indicate the coordination of the monocarbaborate cages $[CB_{11}H_{12}]^{-}$ via edges or faces.

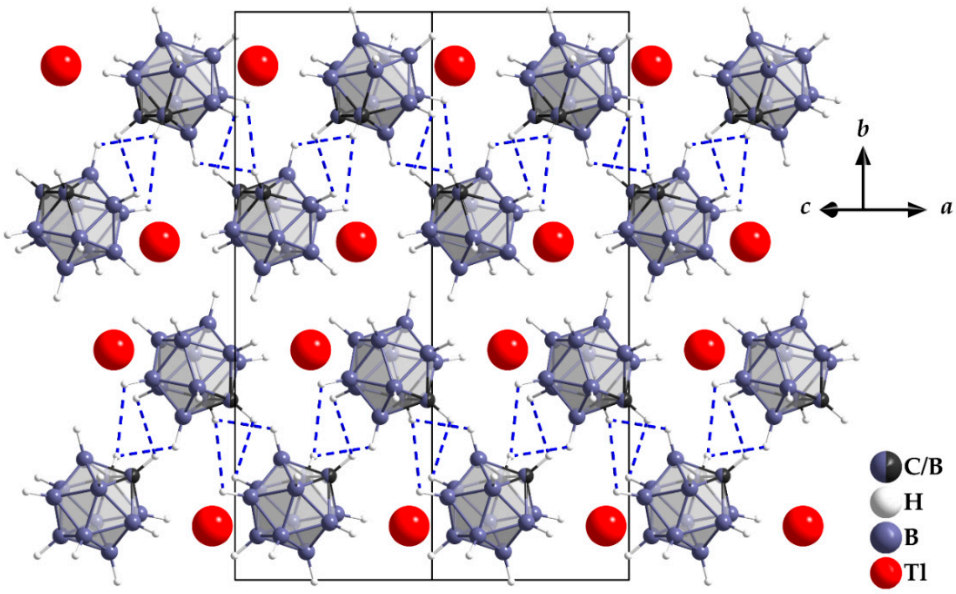

Figure 5. Representation of two extended unit cells of $Tl[CB_{11}H_{12}]$ along [101] with highlighted electrostatic $C^{\delta-}$–$H^{\delta+}$ ··· $^{\delta-}H$–$B^{\delta+}$ interactions.

The already known potassium monocarbaborate $K[CB_{11}H_{12}]$ was reported to crystallize in the space group $P2_1/c$ as well with a = 997.92(6) pm, b = 1967.82(6) pm, c = 998.41(6) pm and β = 93.267(2)° for eight formula units per unit cell on basis of ab-initio calculations and Rietveld refinements of X-ray powder diffraction data [2]. According to the shown unit cells in Figure 6, $K[CB_{11}H_{12}]$ crystallizes isostructurally with $Tl[CB_{11}H_{12}]$ as an ordered variant with an enlarged unit cell. Doubling the $P2_1/c$ unit cell of $Tl[CB_{11}H_{12}]$ along the a-axis leads to the one of $K[CB_{11}H_{12}]$ in the $P2_1/n$ setting and then can be transformed into the literature known $P2_1/c$ cell of $K[CB_{11}H_{12}]$ as shown in Figure 7. As we did not find any further reflections indicating a larger unit cell along the reciprocal a-axis in the reconstructed reciprocal diffraction images of $Tl[CB_{11}H_{12}]$ (Figure 8), it can be stated that there is no ordering in our measured single-crystalline specimen of $Tl[CB_{11}H_{12}]$. The decision, whether rotational or orientational disorder is present, would be subject of further temperature-dependent investigations. The rotational disorder of the $[CB_{11}H_{12}]^-$ anion around a *pseudo*-twofold axis, however, mimics roughly the structural arrangement of the neutral *closo*-dicarbadodecaborane *o*-$[C_2B_{10}H_{12}]$ (1,2-$[C_2B_{10}H_{12}]$: monoclinic, *Pc*) [17].

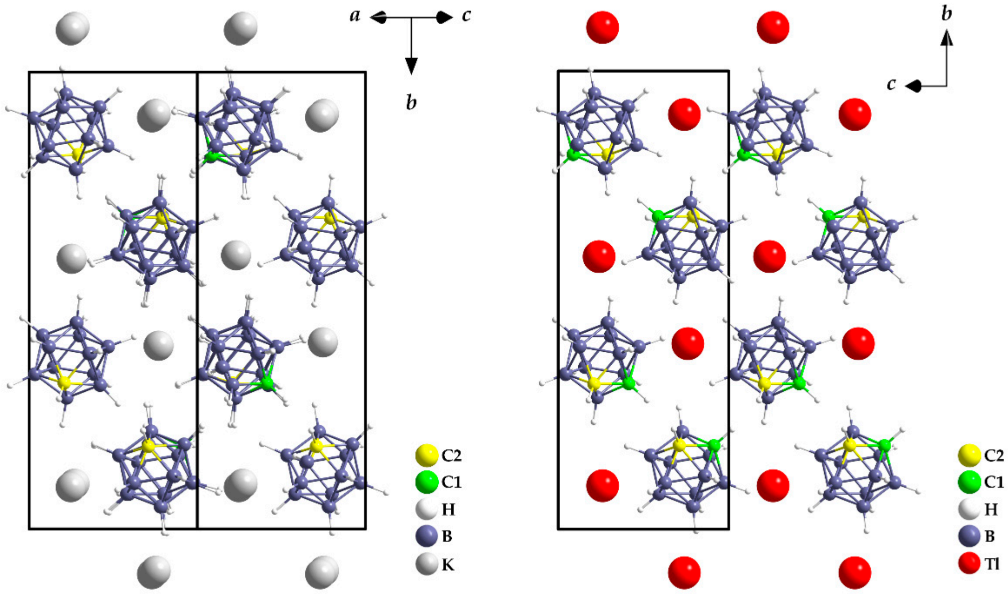

Figure 6. Comparison of the ordered $K[CB_{11}H_{12}]$ (**left**) and the disordered $Tl[CB_{11}H_{12}]$ structure (**right**), showing that the determined positions of C1 and C2 are the same for both monoclinic arrangements after superimposition.

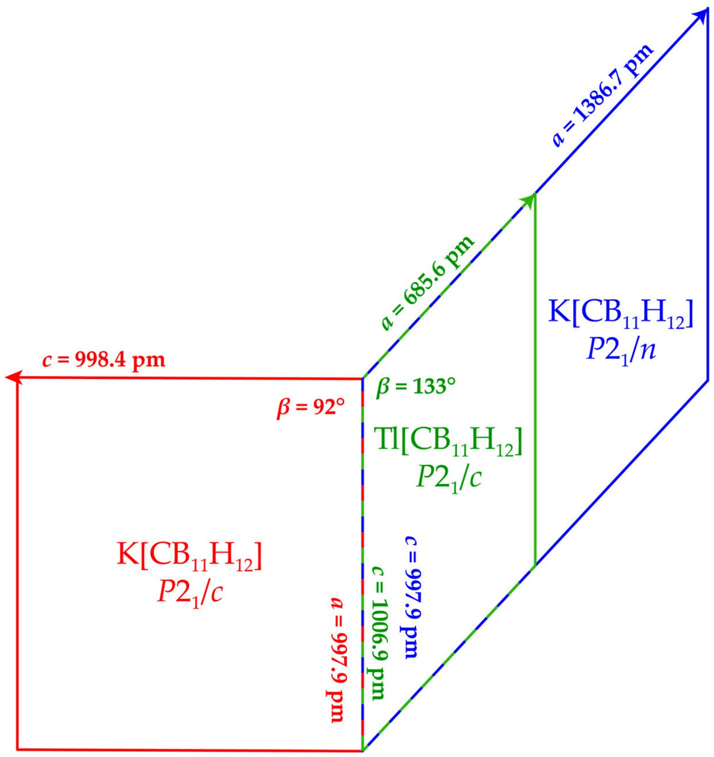

Figure 7. Symmetry relationship of the monoclinic unit cells of the literature-known $K[CB_{11}H_{12}]$ [2] (red and blue) and the new $Tl[CB_{11}H_{12}]$ (green).

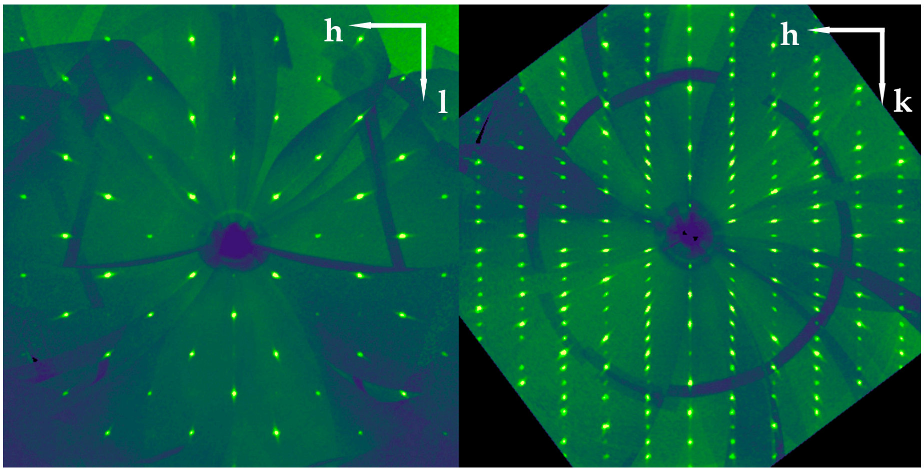

Figure 8. Reconstructed reciprocal diffraction images of $Tl[CB_{11}H_{12}]$, indicating no further *h* values that would lead to an ordering of the carbon-atom sites in the crystal structure of $Tl[CB_{11}H_{12}]$.

3.2. Raman Spectrum

The single-crystal Raman spectrum of $Tl[CB_{11}H_{12}]$ (Figure 9) appears almost identical to the known Raman spectrum of $Cs[CB_{11}H_{12}]$ already described in the literature [3,18]. A sharp band with slight splitting can be seen at 3047 cm^{-1}, which originates from the C–H valence vibration [19]. This confirms the presence of carbon in the dodecaborate cage and also supports the assumption of alternating occupation of the C1 and C2 positions. Subsequently, in the region of the asymmetric breathing vibration of the carbaborate cage from 2600 to 2400 cm^{-1}, a splitting into several signals at 2583, 2563 and 2517 cm^{-1} is observed. On the basis of density functional theory calculations, the interaction-free carbaborate anion $[CB_{11}H_{12}]^-$ should even show seven different B–H stretching vibrations or vibration combinations according to its ideal C_{5v} symmetry [18]. In the solid state and coordinated to cations, both further splitting or reduction of the number of bands is possible. Next, from 1200 to 850 cm^{-1}, the B–H and C–H bending-vibration area can be observed, which is followed by the symmetric breathing mode of the carbaborate cage at 758 cm^{-1} as most intense and sharp band in the whole spectrum. Subsequently, several B–B and C–B bending vibrations from 726 to 490 cm^{-1} and finally the phalanx of lattice vibrations at 55 cm^{-1} with a shoulder extending up to 140 cm^{-1} are encountered.

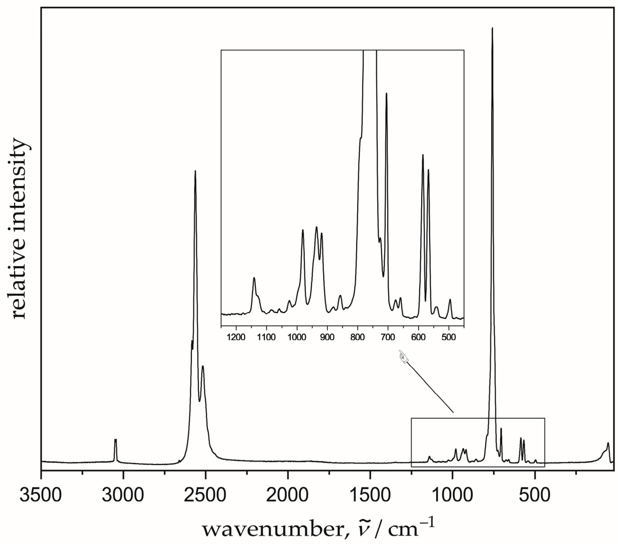

Figure 9. Single-crystal Raman spectrum of $Tl[CB_{11}H_{12}]$ recorded at an excitation wavelength of λ = 532 nm.

3.3. Optical Spectra

The reflection spectrum of a $Tl[CB_{11}H_{12}]$ sample (Figure 10) shows a high reflectance over most of the visible range, which is in line with the observation of a white body color of the microcrystalline powder. From the blue to violet range, the reflectance starts to decline, whereby over the whole UV range a broad unstructured absorption appears, which is assigned to absorption processes attributed to Tl^+. A weaker shoulder at about 420 nm is visible, too, in which the origin may be caused by Urbach tailing (i.e., structural defect related absorption processes) [20].

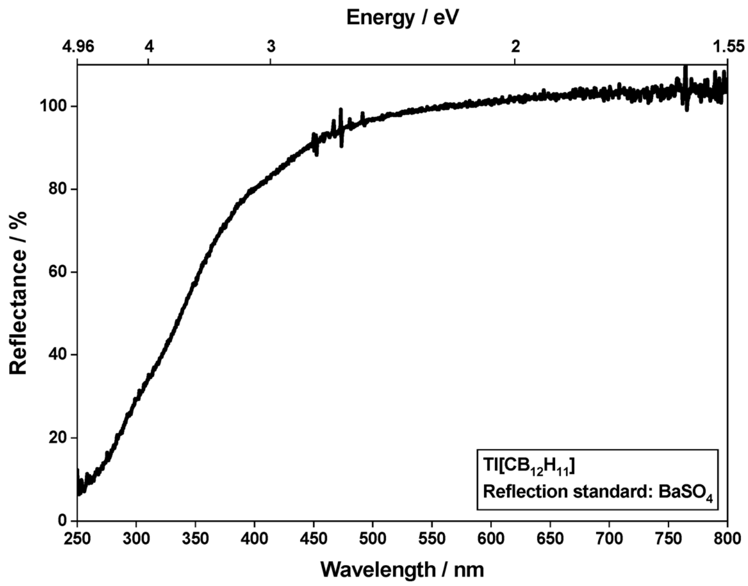

Figure 10. Reflection spectrum of a microcrystalline $Tl[CB_{11}H_{12}]$ sample versus the white reflectance standard $Ba[SO_4]$.

The emission spectrum (Figure 11) upon excitation with UV radiation (280 nm) shows a broad-band peaking at 410 nm (23800 cm^{-1}) with a pretty large full width at half maximum of about 6200 cm^{-1} and a tailing at the low energy edge, which extends to about 600 nm (16700 cm^{-1}).

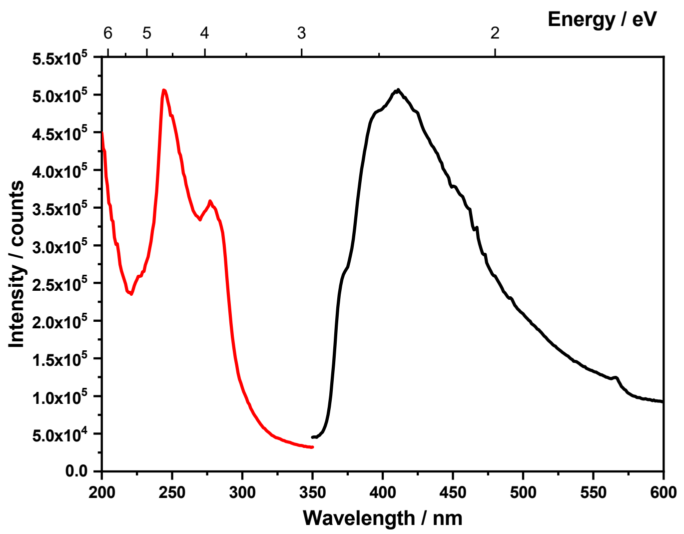

Figure 11. Room-temperature emission spectrum (black) under 280 nm excitation and the excitation spectrum (red) monitored at 420 nm of a white powder sample of $Tl[CB_{11}H_{12}]$.

It is assumed, that the photoluminescence process is caused by an interconfigurational $[Xe]4f^{14}5d^{10}6s^2$ ($^1S_0$) to $[Xe]4f^{14}5d^{10}6s^16p^1$ (^3P_J) transition (lone-pair luminescence) of Tl^+. The detailed interpretation of the Tl^+ luminescence was delivered by Seitz a long time ago [21]. He described the ground state of the free Tl^+ ion as a non-degenerated singlet term $^1S_0$ while the excited states are assigned as spin-orbit levels of the triplet term, viz. $^3P_0$, $^3P_1$, and $^3P_2$, as well as the singlet term $^1P_1$ in sequence of increasing energy [21,22]. In view of the energy levels mentioned before, the strong excitation bands at 245 nm (40800 cm^{-1}) and 280 nm (35700 cm^{-1}) are assigned to the $^1S_0 \rightarrow {}^3P_2$ and $^1S_0 \rightarrow {}^3P_1$ transitions of Tl^+, while the strong spin-orbit coupling in the case of the Tl^+ cation lifts the spin-selection rule on these transitions [22]. The broad emission band and the large Stokes shift of about 11900 cm^{-1} are reasonable for s^2 ions [23].

The fitting of the thermal quenching curve (Figure 12) between 100 and 500 K is done using the formula developed by Struck and Fonger [24–26]; see the equation below. We found that the activation energy E_a of the quenching process is solely 0.097 eV, and thus the quenching temperature $T_{1/2}$ is rather low, viz. at 230 K.

$$\frac{I(T)}{I_0} = \left[1 + Ae^{\frac{-E_a}{k_b T}}\right]^{-1}$$

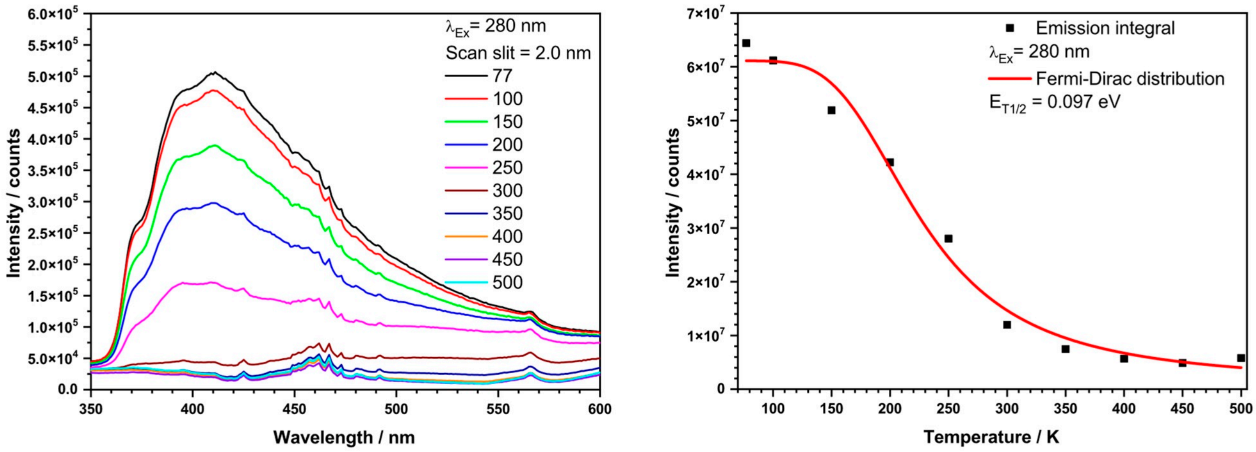

Figure 12. Temperature-dependent emission spectra (**left**) and temperature-dependent emission spectra integrals from 350 to 600 nm (**right**) of $Tl[CB_{11}H_{12}]$ under 280 nm excitation between 100 and 500 K.

Therefore, the photoluminescence is widely quenched at room temperature, and thus the quantum yield at 293 K is lower than 10 %. Such an observation is typically made for s^2-cation activated luminescent materials with a large Stokes shift [23]. Due to the sole moderate signal-to-noise ratio of the emission spectra, the calculation of color coordinates or luminous efficacy values were not considered.

4. Conclusions

The previously unknown thallium(I) dodecahydro-monocarba-*closo*-dodecaborate $Tl[CB_{11}H_{12}]$ was obtained as several millimeters large single crystals from aqueous solution. Its structure could be determined on basis of single-crystal X-ray diffraction data, which showed differences in terms of the carbon-versus-boron positions within the crystal structure as compared to the otherwise isostructural potassium salt $K[CB_{11}H_{12}]$ [2]. Reconstructed reciprocal diffraction images were evaluated to prove the carbon-atom disorder in the crystal structure of $Tl[CB_{11}H_{12}]$. Therefore, Tl^+ cations and $[CB_{11}H_{12}]^-$ anions form a distorted halite-type structure with double layers of $[CB_{11}H_{12}]^-$ cages and intercalated Tl^+ cations. As for the *closo*-carbaborates, the usual hydrogen atoms bound to carbon atoms of the cage stay coordinatively inactive, thus the layers are stabilized by electrostatic C–

$H^{\delta+}\cdots{}^{\delta-}H$–B interactions, which may be referred to as very weak non-classical hydrogen bonds ("dihydrogen bonds").

In terms of optical properties, $Tl[CB_{11}H_{12}]$ shows $6s^2$ lone-pair luminescence with a maximum emission at 420 nm at 280 nm excitation. The quantum yield of less than 10 % at room temperature is rather low and can be explained by the low activation energy for thermal quenching, which is also reflected in temperature-dependent measurements showing maximum emission intensity in a range of 77 to 100 K. Compared to the luminescence properties of the already known related thallium(I) salts $Tl_2[B_{12}H_{12}]$, $Tl_2[B_{10}H_{10}]$ and $Tl_3Cl[B_{12}H_{12}]$, the presented $Tl[CB_{11}H_{12}]$ shows no red shifting of the photoluminescence like $Tl_2[B_{12}H_{12}]$ or $Tl_2[B_{10}H_{10}]$ (emissions at 522 and 510 nm) and has the highest full width at half maximum of 6200 cm^{-1} compared to 4000 to 4700 cm^{-1} of the *closo*-hydroborate salts. In the end, it cannot cope with the strong luminescence properties of $Tl_3Cl[B_{12}H_{12}]$; however, the mixed coordination sphere of chloride and hydridic hydrogen of the $[B_{12}H_{12}]^{2-}$ anions seem to favour strong emission intensity and a high quantum yield (Figure 13) [6,8].

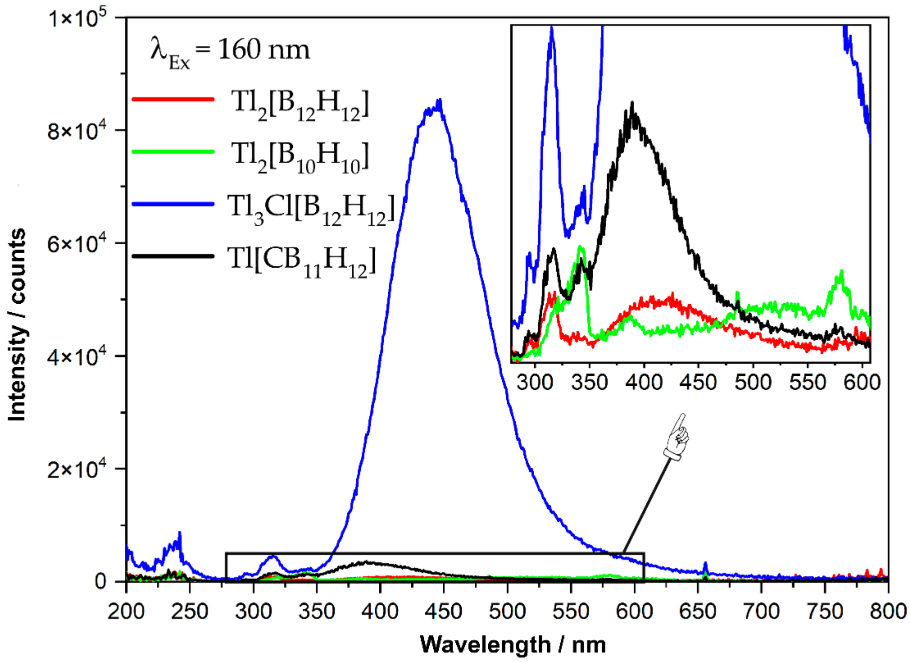

Figure 13. Comparison of the emission spectra of four different thallium(I) *closo*-hydroborates at an excitation wavelength of λ = 160 nm.

Author Contributions: Conceptualization, all authors; methodology, all authors; software, all authors; validation, all authors; formal analysis, all authors; investigation, all authors; resources, all authors; data curation, all authors; writing—original draft preparation, all authors; writing—review and editing, all authors; visualization, all authors; supervision, all authors; project administration, all authors.; funding acquisition, all authors. All authors have read and agreed to the published version of the manuscript.

Funding: This research received no external funding.

Conflicts of Interest: The authors declare no conflict of interest.

References

1. Tang, W.S.; Unemoto, A.; Zhou, W.; Stavila, V.; Matsuo, M.; Wu, H.; Orimo, S.-I.; Udovic, T.J. Unparalleled lithium and sodium superionic conduction in solid electrolytes with large monovalent cage-like anions. *Energy Environ. Sci.* **2015**, *8*, 3637–3645. [CrossRef]
2. Dimitrievska, M.; Wu, H.; Stavila, V.; Babanova, O.A.; Skoryunov, R.V.; Soloninin, A.V.; Zhou, W.; Trump, B.A.; Andersson, M.S.; Skripov, A.V.; et al. Structural and Dynamical Properties of Potassium Dodecahydro-monocarba-*closo*-dodecaborate: $K[CB_{11}H_{12}]$. *J. Phys. Chem.* **2020**, *C 124*, 17992–18002. [CrossRef]

3. Bareiß, K.U.; Friedly, A.; Schleid, T. Die unerwartete Kristallstruktur des Cäsium-Dodekahydro-Monocarba-*closo*-Dodekaborats $Cs[CB_{11}H_{12}]$. *Z. Naturforsch.* **2020**, *75 b*, 1049–1059. [CrossRef]
4. Romerosa, A.M. Thermal, structural and possible ionic-conductor behaviour of $CsB_{10}CH_{13}$ and $CsB_{11}CH_{12}$. *Thermochim. Acta* **1993**, *217*, 123–128. [CrossRef]
5. Černý, R.; Brighi, M.; Murgia, F. The crystal chemistry of inorganic hydroborates. *Chemistry* **2020**, *2*, 805–826. [CrossRef]
6. Bareiß, K.U.; Kleeberg, F.M.; Enseling, D.; Jüstel, T.; Schleid, T. $Tl_2[B_{10}H_{10}]$ und $Tl_2[B_{12}H_{12}]$: Kristallstrukturen, Raman-Spektren und Tl+-Lone-Pair-Lumineszenz im Vergleich. *Z. Naturforsch.* **2022**, *77 b*, 179–187. [CrossRef]
7. Van, N.-D.; Tiritiris, I.; Schleid, T. $Tl_2[B_{12}H_{12}]$: Thallium(I) Dodecahydro-*closo*-dodecaborate with $Cs_2[B_{12}H_{12}]$-Type Crystal Structure. *Z. Anorg. Allg. Chem.* **2004**, *630*, 1764. [CrossRef]
8. Bareiß, K.U.; Bette, S.; Enseling, D.; Jüstel, T.; Schleid, T. Extraordinary intense blue Tl^+ lone-pair photoluminescence from thallium(I) chloride hydroborate $Tl_3Cl[B_{12}H_{12}]$. *Dalton Trans.* **2022**, *51*, 13331–13341. [CrossRef]
9. Sheldrick, G.M. *SHELXS/L-2013, Programs for Crystal Structure Determination*; University of Göttingen: Göttingen, Germany, 2013.
10. Sheldrick, G.M. A short history of *SHELX*. *Acta Crystallogr.* **2008**, *A 64*, 112–122. [CrossRef]
11. Sheldrick, G.M. Crystal structure refinement with *SHELXL*. *Acta Crystallogr.* **2015**, *C 71*, 3–8.
12. Hanson, H.P.; Herman, F.; Lea, J.E.; Skillman, S. HFS atomic scattering factors. *Acta Crystallogr.* **1964**, *17*, 1040–1044. [CrossRef]
13. Crabtree, R.H.; Siegbahn, P.E.; Eisenstein, O.; Rheingold, A.L.; Koetzle, T.F. A New Intermolecular Interaction: Unconventional Hydrogen Bonds with Element–Hydride Bonds as Proton Acceptor. *Acc. Chem. Res.* **1996**, *29*, 348–354. [CrossRef]
14. Klooster, W.T.; Koetzle, T.F.; Siegbahn, P.E.M.; Richardson, T.B.; Crabtree, R.H. Study of the N−H···H−B Dihydrogen Bond Including the Crystal Structure of BH_3NH_3 by Neutron Diffraction. *J. Am. Chem. Soc.* **1999**, *121*, 6337–6343. [CrossRef]
15. Custelcean, R.; Jackson, J.E. Dihydrogen bonding: Structures, energetics, and dynamics. *Chem. Rev.* **2001**, *101*, 1963–1980. [CrossRef]
16. Batsanov, S.S. Bis(but-2-enoato-κO)triphenylbismuth(V). *Inorg. Mater.* **2001**, *37*, 871–885. [CrossRef]
17. Brighi, M.; Murgia, F.; Łodziana, Z.; Černý, R. Structural Phase Transitions in *closo*-Dicarbadodecaboranes $C_2B_{10}H_{12}$. *Inorg. Chem.* **2022**, *61*, 5813–5823. [CrossRef]
18. Kononova, E.G.; Bukalov, S.S.; Leites, L.A.; Lyssenko, K.A.; Ol'shevskaya, V.A. Vibrational spectra and structures of cesium salts with the icosahedral monocarba-*closo*-dodecaborate anion, $[CB_{11}H_{12}]^-$, and its *nido*-derivative, $[CB_{10}H_{13}]^-$ *Russ. Chem. Bull. Int. Ed.* **2003**, 85–92. [CrossRef]
19. Weidlein, J.; Müller, U.; Dehnicke, K. *Schwingungsspektroskopie*, 2nd ed.; Thieme: Stuttgart, Germany, 1988; pp. 142–144. ISBN 978-3-136-25101-0.
20. Urbach, F. The long-wavelength edge of photographic sensitivity and of the electronic absorption of solids. *Phys. Rev.* **1953**, *92*, 1324–1326. [CrossRef]
21. Seitz, F. Interpretation of the Properties of Alkali Halide - Thallium Phosphors. *J. Chem. Phys.* **1938**, *6*, 150–162. [CrossRef]
22. Blasse, G.; Grabmeier, B.C. *Luminescent Materials*; Springer: Berlin/Heidelberg, Germany; New York, NY, USA, 1994; ISBN 978-3-540-58019-5.
23. Ronda, C.R. *Luminescence*; Wiley-VCH: Weinheim, Germany, 2006; ISBN 978-3-527-31402-7.
24. Fonger, W.H.; Struck, C.W. Eu^{3+} ^5D Resonance Quenching to the Charge-Transfer States in Y_2O_2S, La_2O_2S, and LaOCl. *J. Chem. Phys.* **1970**, *52*, 6364–6372. [CrossRef]
25. Struck, C.W.; Fonger, W.H. Role of the charge-transfer states in feeding and thermally emptying the ^5D states of Eu^{3+} in yttrium and lanthanum oxysulfides. *J. Lumin.* **1970**, *1-2*, 456–469. [CrossRef]
26. Struck, C.W.; Fonger, W.H. Thermal Quenching of Tb^{3+}, Tm^{3+}, Pr^{3+}, and Dy^{3+} $4f^n$ Emitting States in La_2O_2S. *J. Appl. Phys.* **1971**, *42*, 4515–4516. [CrossRef]